Soft Matter

ROYAL SOCIETY
OF CHEMISTRY | Celebrating IYPT 2019

PAPER
Leela Rakesh, Shashi P. Karna, George John *et al.*
Freestanding organogels by molecular velcro of
unsaturated amphiphiles

Soft Matter

PAPER

Freestanding organogels by molecular velcro of unsaturated amphiphiles†

Vijai Shankar Balachandran,‡§[a] Kizhmuri P. Divya,‡[a] Malick Samateh,[ab] Sai S. Sagiri,[a] Sitakanta Satapathy,[a] Padmanava Pradhan,[a] Srinivasa R. Raghavan, [c] Leela Rakesh,*[d] Michael S. Sellers,[e] Shashi P. Karna*[e] and George John [*ab]

A simple amphiphile, *N*-cardanyltaurine amide (NCT) with different degrees of *cis*-unsaturation in its tail resulted in the formation of strong organogels. Interestingly, this is in contrast to the commonly accepted notion that introducing unsaturation in alkyl chains enhances fluidity in lipid assemblies. The physico-chemical and first-principles DFT calculations confirmed the pegging of 'kinked' unsaturated side chains, where the hydrophobic interlocking as in Velcro fasteners leads to a network of cylindrical micelles, resulting in self-standing organogels. Textural profile analysis and spectroscopic details substantiated the dynamic assembly to resemble a 3D network of gelators rather than being a cross-linked or polymerized matrix of monomers.

[a] *Department of Chemistry and Biochemistry and Center for Discovery and Innovation, The City College of New York, 85 St. Nicholas Terrace, New York, NY 10031, USA. E-mail: gjohn@ccny.cuny.edu*

[b] *Doctoral Program in Chemistry, The City University of New York Graduate Center, 365 5th Avenue, New York, NY 10016, USA*

[c] *Department of Chemical and Biomolecular Engineering, University of Maryland, College Park, MD 20742, USA. E-mail: sraghava@umd.edu*
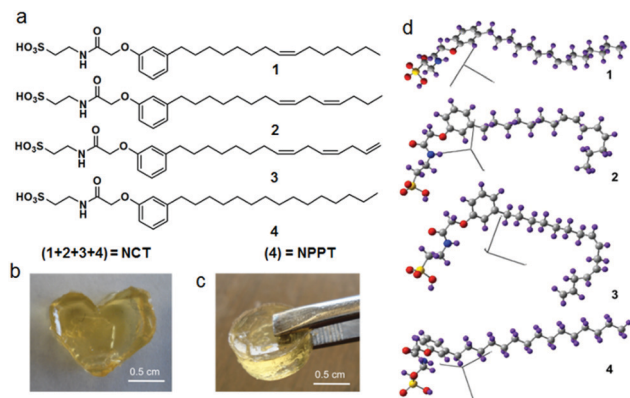
[d] *Department of Mathematics, Central Michigan University, Mount Pleasant, MI 48859, USA. E-mail: leela.rakesh@cmich.edu*

[e] *Army Research Laboratory, Weapons & Materials Research Directorate, Aberdeen Proving Ground, MD 21005, USA. E-mail: shashi.p.karna.civ@mail.mil*

† Electronic supplementary information (ESI) available: Computational details, rheology and SANS, ^{2}H NMR studies, optical polarizing microscopic studies, gelation studies, molecular simulations, textural profile analysis, DPD Simulation. See DOI: 10.1039/c9sm00378a

‡ These authors contributed equally to this work.

§ Present address: Advanced Analytical Sciences, Reliance Research & Development Centre, Navi Mumbai 400701, India.

Introduction

Materials from nature such as bone, skin, nacre and wood exhibit multiple levels of hierarchical structures at the nano and microscale, to impart intricate functionality.[1,2] Such a multilevel hierarchy has been replicated in biomimetic materials that exhibit adhesion to dry surfaces or superhydrophobicity.[3,4] Exploring the fundamental interactions in natural systems has enhanced our understanding at the molecular level and provided clues to replicate the same in generating new functional materials.[5] One such interesting phenomenon is the interlocking of hook-like structures, widely observed in nature. The adhesion of Cocklebur (*Xanthium strumarium*) seeds, Velcro®, and colonies of *Aztecaandrae* ants[6,7] are some examples where

hooking plays an important role in their survival. Nanoscale structures with hooked morphology have shown mechanical interlocking and exhibit adhesion and resilience properties.[8,9] Observation of these interesting systems for such fascinating phenomena has motivated us to explore whether such interlocking can be mimicked *via* molecular interactions for bioinspired self-assembled materials.

One thrust area of our research is the synthesis and assembly of unsaturated amphiphilic molecular systems.[10] Molecular kinks in lipid tails ascribed to $-C=C-$ *cis*-unsaturations[11] are known to be a key factor in dictating the packing of lipids in cell membranes,[12,13] which is imperative for fluidity.[14,15] It is demonstrated that kinks in lipids arising from *cis*-double bonds could dictate the assembly of interlocked bilayers.[16] Herein, we report the formation of molecular gels from a simple amphiphile, *N*-cardanyltaurine amide (NCT)[11] (Fig. 1a) which possesses *cis*-unsaturations in its tail. NCT forms reverse assemblies in organic solvents to form self-standing organogels with enhanced yield strength compared to that of their saturated counterpart. As shown in Fig. 1, organogels of NCT in diesel or toluene (2.0 wt%) are freestanding and moldable.

Results and discussion

NCT was synthesized from cardanol, a byproduct of the cashew industry. Cardanol is a biobased non-isoprene lipid obtained by thermal treatment of cashew nut shell liquid (CNSL). It consists of a rich mixture of phenolic lipids: 5% of 3-(pentadecyl)phenol, 49% of 3-(8*Z*-pentadecenyl)phenol, 17% of 3-(8*Z*,11*Z*-pentadecadienyl)-phenol and 29% of 3-(8*Z*,11*Z*,14-pentadecatrienyl)phenol.[17]

Fig. 1 (a) Molecular structures of *N*-cardanyltaurine amide (NCT) and *N*-pentadecylphenyltaurine amide (NPPT); (b) NCT (2.0 wt%) gel in diesel; (c) NCT (2.0 wt%) gel in toluene; (d) optimized structures (B3LYP/6-31-G) with respective Cartesian axes of NCT showing kinked side chains (red = O, grey = C, blue = N, yellow = S, purple = H).

Thus NCT exists as a mixture of different types of C_{15} tail with one, two, three, or no *cis*-unsaturations. The molecule with no unsaturation is denoted as *N*-pentadecylphenyltaurine amide (NPPT). The minimum gelation concentration (MGC) of NCT ranged from 1 to 2 wt%, depending on the solvent (Table S1, ESI†). In all cases, gelation was found to be thermo-reversible.

Experimental characterization of NCT gels

The NCT gels showed that the storage modulus G' was independent of frequency and much higher than the loss modulus G'' over the frequency range (Fig. 2a and Fig. S3a, ESI†). This response is typical of a molecular gel, as it indicates that the sample does not relax over long time scales. The G' value for NCT gel was about 1000 Pa. The value of the dynamic yield stress σ_y is 100 Pa, which is relatively high, and consistent with the freestanding nature of the gel.

Small-angle neutron scattering (SANS) showed a q^{-1} dependence of the scattering intensity at low q, suggesting the presence of cylindrical assemblies in the organogels (Fig. 2b). The formation of such reverse micellar self-assemblies is fascinating and unfortunately, studies on such systems have been rarely carried out in other media except water.[18–25] The Guinier plot ($\ln[Iq]$ *vs.* $[q^2]$) yielded an estimate of the chain diameter of ~ 4.6 nm which is twice the average length of an NCT molecule.
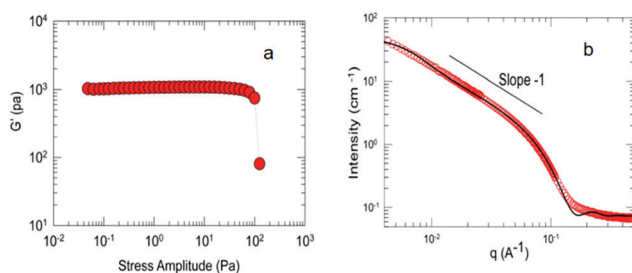
Fig. 2 (a) Stress sweep dynamic rheology profile of the NCT gel showing a yield stress of ~ 100 Pa, (b) small angle neutron scattering (SANS) of 2.5 wt% NCT gel in d_8-toluene.
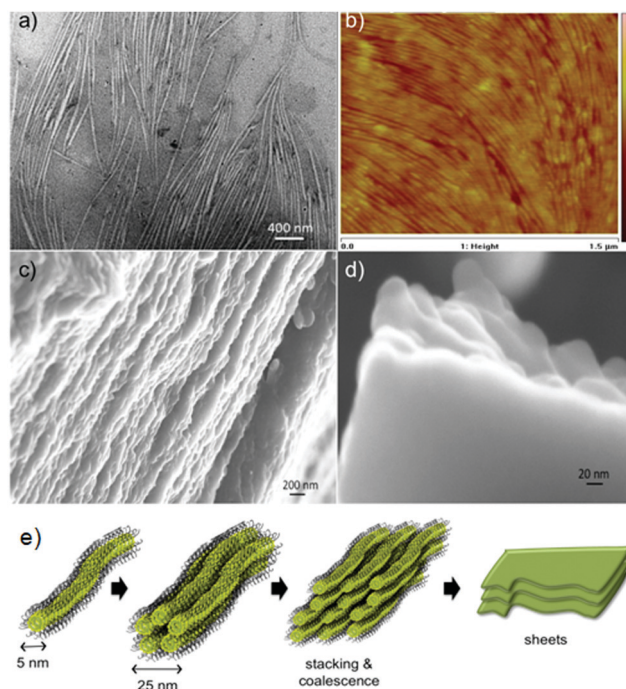
Fig. 3 (a) TEM image of a 2.0 wt% NCT toluene gel; (b) AFM image of a 2.0 wt% NCT butanol gel; (c) SEM image of a 2.0 wt% toluene gel. (d) Stacked sheet-like morphology at higher magnification; (e) schematic of drying induced structure transformation.

The end-to-end length of the chains is expected to be > 100 nm and it cannot be accurately estimated from the SANS data because it falls outside the window of length scales probed by SANS. Based on the amphiphilic structure, NCT is expected to form reverse micelles. The formation of reverse micelles was also confirmed by the ability of NCT gels in toluene to entrap polar rhodamine-6G hydrochloride (Fig. S1a, ESI†).

TEM analysis of the gel showed smooth spaghetti-like cylindrical structures ~ 25 nm in diameter and several micrometers in length (Fig. 3a). AFM analysis also corroborated similar self-assembled structures in the gels (Fig. 3b). These results suggest that the reverse worm-like cylindrical structures (~ 5 nm in diameter) are clustered together *via* hydrophobic unsaturated tails interlocking to form a larger assembly of ~ 25 nm. The SEM images of the xerogel showed stacked sheets 20–35 nm thick (Fig. 3c and d). Such 2D sheets are expected to be formed by the coalescence of the larger assemblies, see Fig. 3e, facilitated by the reduction in surface tension during phasing out (gelation). Such a mechanism of fusing fibrous bundles into sheets has been reported in cross-linked actin and myosin systems,[26] and peptide self-assemblies[27] where membranes with curved geometries are formed due to Rayleigh instabilities.[28] The formation of a freestanding gel induced by hydrophobic interlocking of unsaturated alkyl chains is not reported in the literature.

Mesoscale modeling and simulation of reverse cylindrical structures

DPD (Dissipative Particle Dynamics) simulations were used to probe the rationale behind the formation of a worm-like
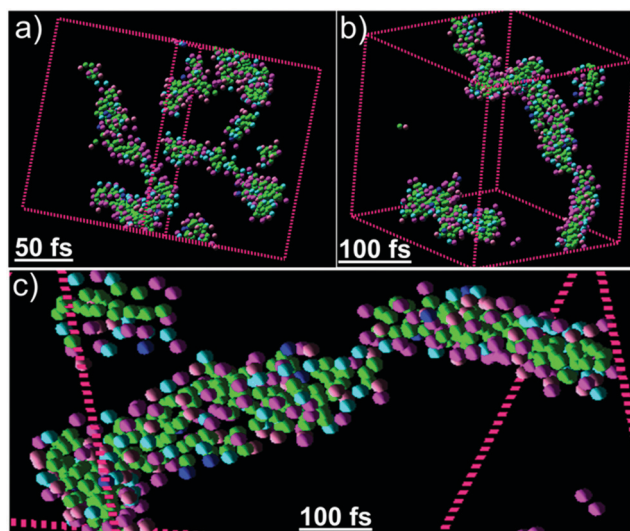
Fig. 4 Snapshots collected from DPD simulation after (a) 50 fs and (b) 100 fs, depicting shorter and longer worm-like micelles, respectively. (c) A selected area snapshot after 100 fs accounting for the reverse micellar cylindrical assembly, where the hydrophilic H-beads (green) and the hydrophobic T-beads (other colors) are mostly projected inward and outward, respectively. [Course grain model details: $-SO_3H$ side head bead (H): green, phenyl + alkyl chain tail bead (T) of D_0: pink, D_1: blue, D_2: sky blue and D_3: magenta, where D_n's represent the respective amphiphiles with 'n' accounting for different degrees of cis-unsaturation. Toluene beads are excluded for clarity purpose. Time evolution of potential energies along with snapshots collected at different timescales and NCT: toluene compositions are provided in Fig. S11, ESI†].

Fig. 5 (a) Plot of interaction energy (kcal mol^{-1}) with respect to frozen carbon atom (C1–C1) separation distances for all ten combinations of saturated/unsaturated alkyl chains in the NCT mixture. Data sets are labeled as C15_X, where X is the number of double bonds in the alkyl chain. The pairs which resulted in unique structures are highlighted in green, yellow, blue, and magenta. The error bars represent the standard deviation of three independent simulations at each point. Alkyl chain pair configurations at ∼18.0 Å after MD simulation; (b) "diene" + "diene", (c) "triene" + "triene" and (d) "monoene" + "triene" pairs. Red spheres indicate end locations of frozen carbon atoms and green cylinders indicate unsaturated C–C bonds.

assembly for NCTs in toluene.[29] The mesoscopic course-grain (CG) model (NCTs + toluene) for simulation under boundary condition was considered to be composed of three beads, where the hydrophilic and hydrophobic components of NCTs were the head (H) and tail (T) beads, respectively, while toluene as the solvent was considered to represent a single bead (simulation details are provided in the Computational section, ESI†). The simulation results at 313 K revealed that the NCT beads in toluene gradually self-assemble from short (Fig. 4a) to relatively long (Fig. 4b) worm-like cylindrical chains as the system approaches the equilibrium state at higher timescales (Fig. S7 and S9, ESI†). The hydrophilic ($-SO_3H$ side) H-beads and the hydrophobic (alkyl chain and phenyl groups) T-beads radially project in and out respectively, accounting for the reverse micellar assembly, see Fig. 4c. The micellar worm-like assembly was consistent for two different NCT:toluene bead compositions (Fig. S7 and S11, ESI†), validating the AFM and TEM results shown in Fig. 3.

To further investigate the interactions responsible for "pegging" of the kinked hydrophobic chains, molecular dynamics (MD) simulations and first-principles density functional theory (DFT) calculations were performed (computaional details, ESI†). The interacting alkyl chain components of the NCT derivatives were considered exclusively for simulations in order to reduce the computational cost. A sum total of 10 pairs of saturated/unsaturated C_{15} lipid chains ("monoene" + "monoene", "monoene" + "diene", "diene" + "diene" and so on) with the

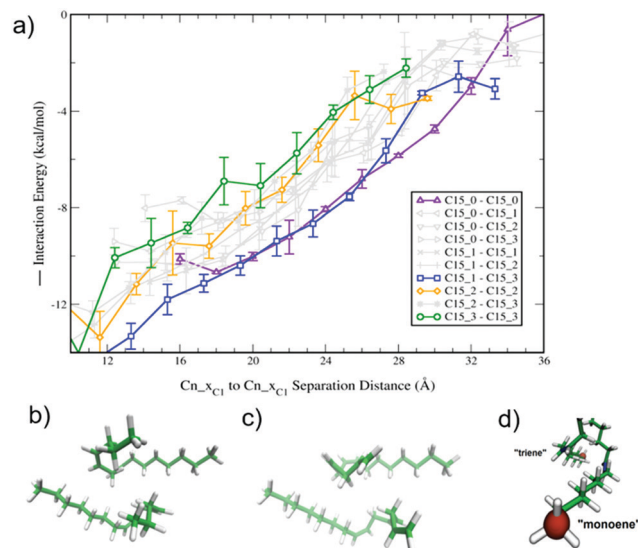number and location of double bonds similar to those of the NCT amphiphiles were constructed. The respective energies were calculated at C_1–C_1 separation distances ranging from ∼10.0 to ∼30.0 Å using NAMD molecular dynamics with the CHARMM36 force field.

The interaction energies as a function of distance for all the constructed pairs are shown in Fig. 5 and Table S2 (ESI†). Fig. 5 shows four pairs, i.e., (1) "triene" + "triene" (green); (2) "diene" + "diene" (yellow); (3) "monoene" + "triene" (blue); and (4) "saturated" + "saturated" (magenta) of interest. The calculations reveal that the interaction energies are significantly high for pairs (1) and (2), however relatively low for (3) and (4) over the distances. Pairs (1) to (3) exhibit a moderate amount of interlocking. As expected, pair (4) did not exhibit any interlocking and the saturated alkyl chains remain parallel to one another. These results suggest that chain–chain interlocking could stabilize the pairs of unsaturated chains while compensating for the loss of interaction energy. It is noteworthy to mention that the NCT chains comprise 50% and 29% of "monoene" and "triene", respectively.

From the above studies, we suggest the following mechanism to account for the formation of self-sustainable strong organogels. In non-polar solvents, NCT forms reverse cylindrical micelles with the polar $-SO_3H$ group at the core and the alkyl tails projecting outwards into the solvent. These long micellar assemblies entangle through the solvent to form a 3-D network, resulting in gelation. Due to the kinks in its unsaturated tails, an
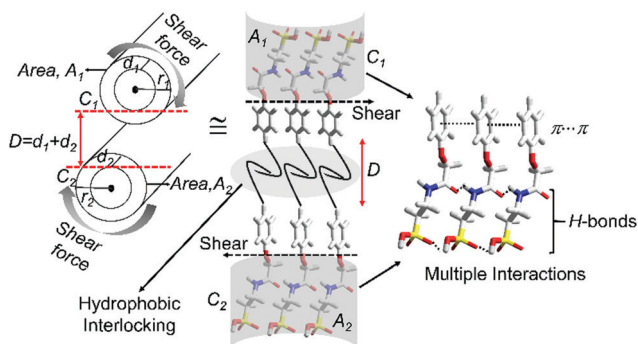
Scheme 1 Schematic showing the geometric models and parameters describing the interactions between the worm-like micelles and the contributing non-covalent forces.

additional type of interaction, *i.e.*, the interlocking of *cis*-unsaturated chains is also observed. When two NCT micellar chains approach each other, the kinked alkyl tails on the exterior of each chain peg with respect to each other at the overlapping points (Scheme 1) to form a network. This velcro-like interlocking strengthens the junction points in the micellar network and thus accounts for the significantly high strength of the NCT gels. Interestingly, the long cylindrical micelles of NCT showed the aligning capability of small organic molecules (Fig. S4, ESI†) such as toluene in the gel state similar to the strain induced alignment (SAG) of CDCl$_3$ in stretched polymeric structures.[30]

Modeling of the Velcro-like interlocked cylindrical structures

We propose a model in order to understand the inter-locking mechanism, as shown in Scheme 1. The model consists of two cylindrical filaments of NCT, *i.e.*, C_1 and C_2, with radii r_1 and r_2, interacting along length l. The areas of contact of C_1 and C_2 are given by A_1 and A_2 (shaded grey area, Scheme 1), respectively. A bilayer of molecular leaflets interacting in a slip-stacked manner through van der Waals and dispersive forces exists in between A_1 and A_2. The average length of overlap between the leaflets is D and their interaction is controlled by the molecular density at the respective areas A_1 and A_2, which in turn maximizes the interlocking at the junctions. The frictional coupling and shear forces between the leaflets (hemifusion under the bilayer model) are controlled by the extent of inter-digitation between them and the viscosity of the solvent.[31] Hemifusion depends on the force per unit area and the inter-leaflet frictional coefficient, which is enhanced by the inter-digitation between the alkyl chains (leaflets) and thus strengthens the shear force due to the asymmetry created by the short and long alkyl chain lengths.[32] The effective decrease in chain length and pegging result from the kinks of *cis* double bonds. This enhances the interlocking across D, imparting high shear strength to the gel.

In addition to the interlocking, the high shear strength of the gel is further attributed to multiple interactions, *e.g.*, the directional H-bonding between amides and carbonyls and π–π stacking of the aromatic cores. The hydrophobic pegging and the hydrogen bonding are orthogonal with respect to each

other, which imparts a significantly high shear strength to the gel.

Studies on hydrodynamic forces between brush-like polymers show that, at distances $D < l/2$, the interpenetrating chains behave like 'solids' with increased relaxation time of the chains.[33] Coarse-grain (CG) modeling of polymer brushes with DPD methods shows entanglement of chains in solvents of identical polarity resulted in an increase in friction. These models provide useful information on the elasticity and minimum distance for effective interaction. These are based on the classic Flory's polymer brush model, which is extended to lipid bilayers with an inverse cube dependence of surface pressure per alkyl chain. The alkyl chains here are equivalent to the structureless polymer chains with confined solvophobic forces.[34]

Cardanol-derived amphiphiles exhibit interesting self-assembly properties.[11,35] To self-assemble in a given solvent medium (differing in terms of their hydrophilic heads), their hydrophilic counter-part provides significant driving force (H-bond and solute–solvent interactions) governed by the packing factor.[36] Rigid glucoside head groups attached to the cardanol moiety form either helical self-assemblies or lipid nanotubes whereas the flexible taurine-derived head group in the present case prefers a truncated conical structure (the critical packing factor [CPP] < 1/2) leading to a cylindrical micellar self-assembly. Further in the present case, the collective hydrophobicity of the cardanol moiety, with varying *cis* –C=C, provided the appropriate hydrophobicity to form gels. We believe that this results in interlocking/pegging of the incoming NCT amphiphile instead of an interdigitated fashion of forming bilayers. The repercussion of this phenomenon is also evident from the interaction energies of various *cis* –C=C pairs as shown in Fig. 5a. This also suggests that the freestanding nature of the gel is dependent on the number of such strong "interlocking densities" which would be further explored in our future studies. Due to the formation of reverse bilayers by cardanol derivatives with glucoside head groups, they do not form very strong gels in toluene as in the case of NCT.

If the above mechanism explains the freestanding ability and strength, then removal or absence of kinks in the molecular structure should disfavor the formation of the interlocks and hence the secondary network. Therefore, one would expect a weak molecular non-self-standing gel. To prove this, a fully saturated derivative of NCT, termed as NPPT (Fig. 1), was synthesized as a control molecular system and tested to determine its gelation behavior. NPPT being an amphiphile, also formed molecular gels, but not free-standing ones (Fig. S2, ESI†). A 2.0 wt% NPPT gel in toluene had a storage modulus (G') of ~36 Pa (Fig. S2, ESI†), which is about 30 times lower than that of a 2.0 wt% NCT gel in toluene (G' ~ 1000 Pa). Moreover, the yield stress (σ_y) of the NPPT gel was only ~4.0 Pa (Fig. S2, ESI†), which is 25 times lower than the σ_y (~100 Pa) of the NCT gel. NPPT gels are paste-like and not freestanding or moldable. Polarizing optical microscopy investigations of the NPPT gels showed highly birefringent fibrillar gels, whereas the NCT gels were non-birefringent (Fig. 6). Thus, the absence of unsaturation in the tail of the amphiphile significantly changes the self-assembly.
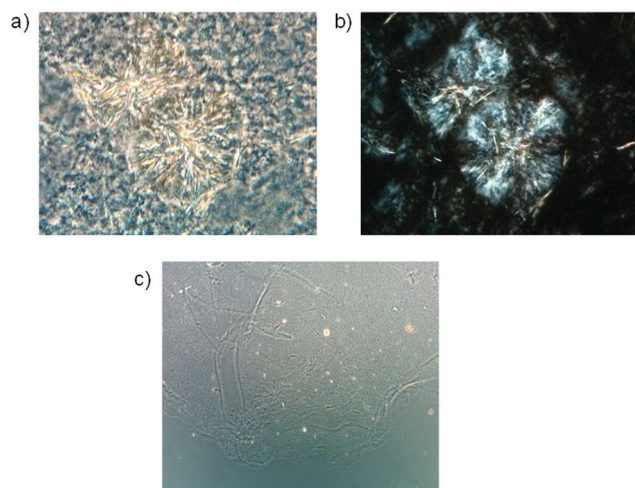
Fig. 6 (a) Phase contrast optical image of NPPT gel in toluene, (b) cross polarized images of NPPT in toluene and (c) cross polarized optical image of NCT in toluene. The NPPT formed birefringent structures in toluene whereas the NCT gel is non-birefringent (magnification 20×).

The physical properties of NCT gels were further evaluated by textural profile analysis (TPA) for large deformations (Fig. S5, ESI†). The hardness of the NCT gel was found to be 0.68 N with high cohesiveness (48.9%) compared to adhesiveness (0.07 N mm) suggesting that the gel could be self-standing. Attempts to perform TPA on the NPPT gel proved futile as they could not generate any textural curve attributed to its weak viscoelastic nature.

Conclusions

In summary, we shed light on a rarely explored phenomenon which describes significantly strong organogelation behavior attributed to the hydrophobic interlocking of *cis* double bonds contributed by a simple amphiphilic system, NCT. The fully saturated control derivative of NCT, *i.e.*, NPPT also results in gelation, however significantly weak in terms of its strength. From SANS, microscopy and simulation studies, we infer that the amphiphiles self-assemble into cylindrical chains of reverse micelles, where the strong gelation ability is attributed to the formation of 3D networks by these chains. Our mesoscale modeling and simulation of NCT in organic solvents proves that additional contribution to significantly high sustainability and mechanical strength of NCT gels stems from the kinked tails of NCT that peg onto each other forming a Velcro-like hooking. This in turn strengthens the junctions between the micellar chains which rationalizes the stronger networks formed in the case of NCT.

Conflicts of interest

There are no conflicts to declare.

Acknowledgements

Notes and references

1 L. B. Smith, T. E. Schäffer, M. Viani, J. B. Thompson, N. A. Frederick, J. Kindt, A. Belcher, G. D. Stucky, D. E. Morse and P. K. Hansma, *Nature*, 1995, **399**, 761–763.

2 A. Al-Amoudi, D. Castaño Díez, M. J. Betts and S. F. Achilleas, *Nature*, 2007, **450**, 832–839.

3 H. Lee, B. P. Lee and P. B. Messersmith, *Nature*, 2007, **448**, 338–341.

4 A. K. Geim, S. V. Dubonos, I. V. Grigorieva, K. S. Novoselov, A. A. Zhukov and S. Y. Shapoval, *Nat. Mater.*, 2003, **2**, 461–463.

5 B. Dragnea, *Nat. Mater.*, 2008, **7**, 102–104.

6 J. M. Benyus, *Biomimicry: Innovation Inspired by Nature*, William Morrow and Company, Inc., New York, NY, 1997.

7 A. Dejean, C. Leroy, B. Corbara, O. Roux, R. Céréghino, J. Orivel and R. Boulay, *PLoS One*, 2010, **5**, 11331–11338.

8 C. Moissl, R. Rachel, A. Briegel, H. Engelhard and R. Huber, *Mol. Microbiol.*, 2005, **56**, 361–370.

9 H. Ko, J. Lee, B. E. Schubert, Y. L. Chueh, P. W. Leu, R. S. Fearing and A. Javey, *Nano Lett.*, 2009, **9**, 2054–2058.

10 P. K. Vemula and G. John, *Acc. Chem. Res.*, 2008, **41**, 769–782.

11 V. S. Balachandran, S. R. Jadhav, P. Pradhan, S. D. Carlo and G. John, *Angew. Chem., Int. Ed.*, 2010, **49**, 9509–9512.

12 S. M. Sagnella, C. E. Conn, I. Krodkiewska, X. Mulet and C. J. Drummond, *Soft Matter*, 2011, **7**, 5319–5328.

13 G. Lagaly and I. Dékany, *Adv. Colloid Interface Sci.*, 2005, **114–115**, 189–204.

14 A. Brizzi, V. Brizzi, M. G. Cascio, T. Bisogno, R. Sirianni and V. Di Marzo, *J. Med. Chem.*, 2005, **48**, 7343–7350.

15 M. J. McFarland, A. C. Porter, F. R. Rakhshan, D. S. Rawat, R. A. Gibbs and E. L. Barker, *J. Biol. Chem.*, 2004, **279**, 41991–41997.

16 S. M. Sagnella, C. E. Conn, I. Krodkiewska, M. Moghaddam, J. M. Seddon and C. J. Drummond, *Langmuir*, 2010, **26**, 3084–3094.

17 (a) J. H. P. Tyman, *Chem. Soc. Rev.*, 1979, **8**, 499–537; (b) V. S. Balachandran, S. R. Jadhav, P. K. Vemula and G. John, *Chem. Soc. Rev.*, 2013, **42**, 427.

18 S.-H. Tung, H.-Y. Lee and S. R. Raghavan, *J. Am. Chem. Soc.*, 2008, **130**, 8813–8817.

19 K. Sun, R. Kumar, D. E. Falvey and S. R. Raghavan, *J. Am. Chem. Soc.*, 2009, **131**, 7135–7141.

20 N. M. Correa, J. J. Silber, R. E. Riter and N. E. Levinger, *Chem. Rev.*, 2012, **112**, 4569–4602.

21 V. P. Sofía, F. O. Andres and M. P. Gárate, *Curr. Top. Med. Chem.*, 2014, **14**, 774–780.

22 S. Sarkar, P. Choudhury, S. Dinda and P. K. Das, *Langmuir*, 2018, **34**, 10449–10468.

23 R. Urano, G. A. Pantelopulos and J. E. Straub, *J. Phys. Chem. B*, 2019, **123**, 2546–2557.

24 D. Singha, D. K. Sahu and K. Sahu, *J. Phys. Chem. B*, 2018, **122**, 6966–6974.

25 D. Blach, M. Pessêgo, J. J. Silber, N. M. Correa, L. García-Río and R. D. Falcone, *Langmuir*, 2014, **30**, 12130–12137.

26 A. Kakgo, S. Sugimoto, J. P. Gong and Y. Osada, *Adv. Mater.*, 2002, **14**, 1124–1126.

27 S. Zhang, M. A. Greenfield, A. Mata, L. C. Palmer, R. Bitton, J. R. Mantei, C. Aparicio, M. O. de la Cruz and S. I. Stupp, *Nat. Mater.*, 2010, **9**, 594–601.

28 P. Lenz and D. R. Nelson, *Phys. Rev. E: Stat. Phys., Plasmas, Fluids, Relat. Interdisc. Top.*, 2003, **67**, 031502.

29 E. Moeendarbary, T. Y. Ng and M. Zangeneh, *Int. J. Appl. Mech.*, 2009, **1**, 737–763.

30 B. Luy, K. Kobzar and H. Kessler, *Angew. Chem., Int. Ed.*, 2004, **43**, 1092–1094.

31 W. K. den Otter and S. A. Shkulipa, *Biophys. J.*, 2007, **93**, 423–433.

32 A. Galuschko, L. Spirin, T. Kreer, A. Johner, C. Pastorino, J. Wittmer and J. Baschnagel, *Langmuir*, 2010, **26**, 6418–6429.

33 J. Klein., Y. Kamiyama, H. Yoshizawa, J. N. Israelachvili, G. Fredrickson, P. Pincus and L. J. Fetters, *Macromolecules*, 1993, **26**, 5552–5560.

34 W. Rawicz, K. C. Olbrich, T. McIntosh, D. Needham and E. Evans, *Biophys. J.*, 2000, **79**, 328–339.

35 G. John, J. H. Jung, M. Masuda and T. Shimizu, *Langmuir*, 2004, **20**, 2060–2065.

36 R. M. Pashley and M. E. Karaman, *Applied Colloid & Surface Chemistry*, Wiley, NY, USA, 2004, p. 69.

Supplementary Information

Freestanding organogels by molecular velcro of unsaturated amphiphiles

Vijai Shankar Balachandran, Kizhmuri P. Divya, Malick Samateh, Sai S. Sagiri, Sitakanta Satapathy, Padmanava Pradhan, Srinivasa R. Raghavan, Leela Rakesh,* Michael S. Sellers, Shashi P. Karna,* and George John*

Table of Contents   **Page number**

1. Experimental Section

Chemicals and Reagents: Cardanol was obtained by double vacuum distillation of cashew nut shell liquid at (3 ± 4) mm Hg in which the fraction boiling at (220 ± 15) °C was collected. Bromomethylacetate was purchased from TCI America. All the chemicals were of analytical grade and used as received.

Nuclear Magnetic Resonance (NMR): The molecular structure of NCT was determined by ^{1}H and ^{13}C NMR (Vega-300 Varian Inc, USA) and FT-IR (Nicolet 380 FT-IR) spectroscopic techniques. NMR experiments were done on a Vega-600 Varian spectrometer using the WATERGATE program (Varian Inc. USA).

Rheology: Dynamic rheological experiments were performed on an AR2000 stress controlled rheometer (TA Instruments). Samples were run at 25 °C using parallel plate geometry (20 mm diameter). Both frequency and stress sweeps were performed. Frequency sweeps were conducted in the linear viscoelastic regime of each sample, as determined previously by stress-sweep experiments (0 to 100% strain at 1 Hz). The gel was also subjected to a dynamic stress sweep, where the moduli were monitored as a function of the stress-amplitude at a constant frequency of 10 rad/s.

Small Angle Neutron Scattering (SANS): The experiments were done on the NG-7 (30 m) beam line at NIST in Gaithersburg, MD. Neutrons with a wavelength of 6 Å were selected. Three sample-detector distances were used to obtain data over a range of wave vectors from 0.004 to 0.4 Å^{-1}. Samples were studied in 2 mm quartz cells at 25 °C. Scattering spectra were corrected and placed on an absolute scale using NIST calibration standards. The data are shown as plots of the absolute intensity I versus the wave vector $q = 4\pi\sin(\theta/2)/\lambda$, where λ is the wavelength of incident neutrons and θ the scattering angle.

Microscopy: AFM analysis was carried out on Bruker MultiMode 8 AFM. SEM analysis by Supra 55 VP scanning electron microscope on carbon substrates. TEM analysis was carried out on ZEISS 902 transmission electron microscope on carbon coated copper grids.

Textural Profile Analysis: To determine the textural/mechanical properties (hardness, cohesiveness, adhesiveness) of the gels, textural profile analysis (TPA) was performed using texture analyzer (TA.HD*Plus*, Stable Microsystems, UK). TPA involves applying large forces, which causes permanent structural deformation of the material. For TPA, uniaxial compression test, the sample was compressed uniaxially using a cylindrical probe (P/5, stainless steel, diameter: 5 mm) in two consecutive cycles. The cross-head was attached with 5 kg load cell and the probe moved at a test speed of 1 mm/sec to a distance of 5 mm in button mode. The obtained data was analyzed using "Exponent Lite" software provided along with the instrument. The peak force of (peak height after) the first compression cycle represents the hardness or firmness of the gel. Cohesiveness and adhesiveness of the gel were determined as the ratio of the positive work done during the 2nd cycle to that done during the 1st cycle and the negative work done during the 1st cycle, respectively.

2. Computational Details

Dissipative Particle Dynamics (DPD) Simulations: In the present work, structural properties, interfacial density, worm like micelle structure formation, potential energy and their dependence on the respective chemical species concentration and the solvent ratio were investigated in detail by DPD simulation. More specifically, such DPD investigation studied here could shed light on the interfacial behavior in toluene and its influence on the worm like micellization (WLM). The simulation box having dimensions of 36 x18 x 18 (in DPD units), with periodic boundary conditions in all directions are used and simulated in the NVT canonical ensemble (particle number N, volume V, and temperature T) using the DPD module of Accelrys Materials Studio® 5.0. In this simulation, all the units are measured in DPD units unless otherwise specified. Present simulation used the bead spring constant as 4 units and the average bond length is the equilibrium bond length between 0.7 and 0.8, having three DPD units of amplitude noise parameter, which satisfies the fluctuation-dissipation theorem, thus the system reached to an equilibrium temperature. A modified velocity-Verlet algorithm is used to integrate the fluid-particle motion in the system, which is dictated by Newton's 2nd law of motion. Two of the most important properties in DPD must be liquid compressibility and mutual solubility, which determines the properties of the surfactant like materials. For the present application, we used the simplest model consisting of NCT molecules represented by a simple harmonic spring in toluene solvent. The interaction parameters among the head, tail of NCT and toluene are computed via the Blend program in MS studio package. We used MS studio DPD module using velocity -Verlet algorithm, using a velocity correction factor (0.70) with a time step of 2.5 nanoseconds.

DPD Model and Bead Selection Details: The mesoscopic course-grain (CG) model (NCTs+Toluene) for simulation under boundary condition was considered to comprise of three beads, where the hydrophilic ($-SO_3H$ side) and hydrophobic (alkyl tail with phenyl ring) components of NCTs were the head (H) and the tail (T) beads, respectively, while toluene as the solvent was considered to reprsent a single bead. The volume of the hydrophobic tail or hydrophilic head bead of NCT is approximately 230 $Å^3$. The volume of one toluene bead (Tol) containing two toluene molecules is reported to be approximately 184 $Å^3$ However, it is relatively smaller than the volume of the tail or head bead (Fig. S8). Therefore, based on the approximated size and the equal volume principle, the simulated NCT molecules, we selected each of them as T_1H_1 to describe the mesoscopic structure the system where H as the hydrophilic head group and T –hydrophobic bead denotes the tail group of each of the NCT mixture. The course grain model colour codes are represnted as follows: $-SO_3H$ head bead (H): Green, Alkyl tail bead (T) of D_0 : Pink, D_1 : Blue, D_2 : Sky blue and D_3 : Magenta, where D_n's represent the respective amphiphiles with 'n' accounting for different degrees of *cis*-unsaturation. The number of beads of the molecule in the present simulation is computed by dividing its molecular weight by the mass of the toluene molecule **(92.13842).**

COMPASS force field parameters were used in the Molecular mechanics of the software package during the optimization process of the system. The Flory-Huggins, χ parameters, for these beads and the solvent were estimated using atomistic simulation that predicts the mesoscopic structure and particle-particle interaction parameters. All atomistic simulations were carried out in the Blend module of Materials Studio® on a PC at the ambient temperature using COMPASS force-field parameters. The simulation box included 150,000 DPD particles having 3 DPD unit of density. Using the theory of Groot and Rabone, the cut-off radius, r_c, computed was about 7.2 Angstroms, and simulated the system using the time step of 2.5

nanoseconds. The number of iterations for each simulation experiment was set at 5×10^4 time steps, and the average deviation from incompressibility (dimensionless) was always less than 3×10^{-5}. Initially, the system was heated to approximately 338 K to equilibrate the liquid and cooled back to a temperature of 313 K for the production run where the results were recorded accordingly.] The Flory-Huggins interaction parameters, χ_{ij} were translated into the DPD interaction parameters, which is calculated using Groot et. al's theory; $a_{ij}=25+3.57\chi_{ij}$, for each ith and j^{th} particle. The surfactant volume fraction, V_s was between 0.1 – 0.5 percentage, and the volume fractions of toluene and amphiphilic molecules are taken as $V_T= (1 - V_s)/2$.

NAMD Molecular Dynamics and Density Functional Calculations: NAMD molecular dynamics simulations were performed using CHARMM36 force field parameters and explicit solvent model using Carperinelo method 2000 version. Distances were maintained during molecular dynamics by freezing the C_1 carbon atoms of each chain during and the calculations were carried out for 1.0 ns. The geometries of the highlighted pairs were then subject further optimization of their structure using first-principles density functional theory (DFT) calculations. During minimization, the inter- and intra-molecular energy was computed using the B3LYP exchange correlation functional with the 6-31G(d) basis set, as implemented in the GAMESS electronic structure code.
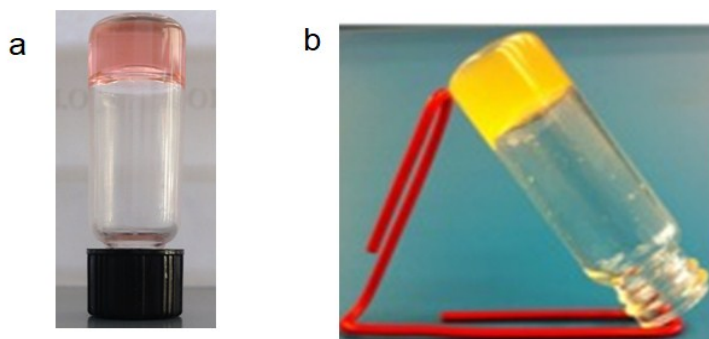
3. **Rheology**

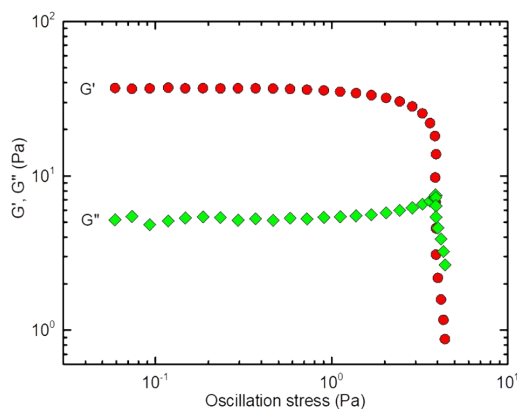Fig. S1. *Photographs of a) NCT with solubilized rhodamine6G in toluene b) NPPT in diesel*

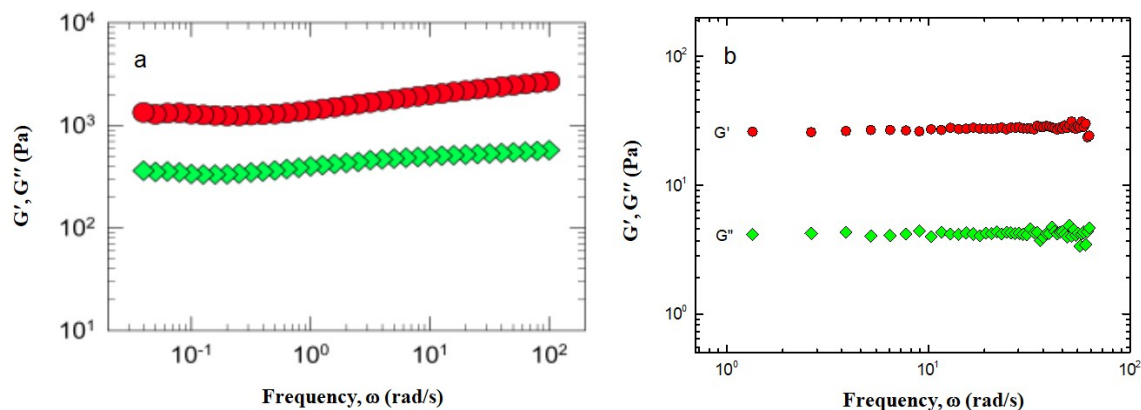

Fig. S2. *Dynamic rheology of 2.0 wt% NPPT gel in toluene*

Fig. S3. *Frequency sweep of 2.0 wt% of a) NCT gel in toluene and b) NPPT gel in toluene*

4. ²H NMR studies
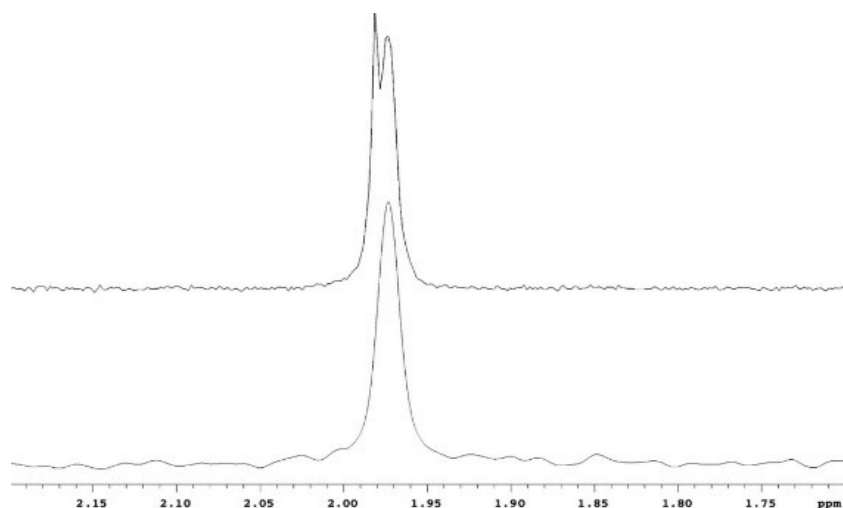

Fig. S4. *²H NMR of toluene gel of NCT grown in a capillary tube. TOP: showing two signals for the residual methyl protons of d_8-toluene. BOTTOM: neat d_8-toluene shown for comparison*

In a typical experiment, an NCT gel (5 wt.%/v) in d^8-toluene was formed in a narrow capillary (2 mm diameter) and its ²H spectrum was recorded. The residual methyl protons of toluene at 2.8 ppm were split suggesting the presence of two magnetically unequivalent –CH₃ protons (of toluene) in the medium. (Fig.S4). A number of material phases such as bicelles,[1] liquid crystals[2] and polymers[3] in organic solvents demonstrate aligning ability when observed using residual dipolar coupling NMR. In the present case, the lengthier worm-like structures of NCT pervade in the gel structure resulting in the hydrophobic interlocks in the equilibrium gel state. The probability of interlocking increases, as the volume available for the growth of 1D reverse worms is highly restricted by the dimensions of the gelation tube. As a result, the worm-like structures experience a situation of maximum hydrophobic interlocks along the long axis of the tube. We speculate that the alignment tensors for the entrapped toluene molecules originate from the

6

strong steric effects provided by the hydrophobic pockets formed due to interlocks as well as from the competing π-stacking with the NCT molecules. Although, there is anisotropy between the two magnetically inequivalent protons, due to weak dipolar coupling, the alignment angle between the d_8-toluene and entrapped toluene is very less. Consequently, the splitting of signals becomes weak.
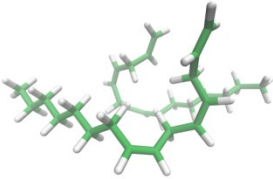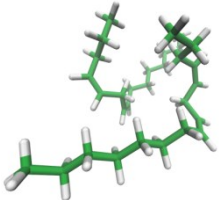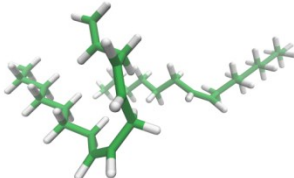
5. **Gelation studies**

Table S1. Gelation characteristics of NCT in various organic solvents (G- Gel; S- Soluble; P- Precipitate)

SOLVENT	RESULT	MGC (wt%)
Hexane	G	1.1
Diesel	G	1.5
Toluene	G	2.0
Water	S	-
2-Butanone	G	1.2
Cyclohexanol	G	1.5
Butanol	G	1.5
Methyl laurate	G	1.2
Heptanone	G	1.2
Cyclohexane	G	1.2
Xylene	G	1.2
Isooctane	P	-

6. Molecular Dynamics (MD) simulations

Table S2. Comparison of interaction energies and visually investigated amount of lipid chain "hooking" from molecular dynamics simulations for each pair of lipids

HOOKING COMBINATION	SNAPSHOT WITH ENERGY	INTERLIPID sp^2 DISTANCE[a]	BOND LENGTHS[b]	
C15_3 + C15_3	B3LYP/N31: -0.00002469 eV	**[L1C$_{15}$-L2C$_{15}$] = 4.665154 Å**	C15_3	0.000154 (C$_8$-C$_9$)
				-0.000022 (C$_{11}$-C$_{12}$)
				0.000410 (C$_{14}$-C$_{15}$)
			C15_3	*0.000051 (C$_8$-C$_9$)*
				0.000651 (C$_{11}$-C$_{12}$)
				0.000130 (C$_{14}$-C$_{15}$)
C15_2 + C15_2	B3LYP/N31: -0.0525 eV	**C15_2 + C15_2** [L1_C$_8$-L2C$_9$] = 5.765706	C15_2	0.000491 (C$_8$-C$_9$)
				0.001919 (C$_{11}$-C$_{12}$)
			C15_2	*0.000063 (C$_8$-C$_9$)*
				0.000914 (C$_{11}$-C$_{12}$)
C15_1 + C15_3	B3LYP/N31: -0.0696 eV	**C15_1 + C15_3** [L1C$_9$-L2C$_{11}$] = 5.608288	C15_1	0.001519 (C$_8$-C$_9$)
			C15_3	*0.000381 (C$_8$-C$_9$)*

[a] The inter-lipid sp^2 distance, e.g., L1C$_x$-L2C$_y$ corresponds to the optimizes distance between the unsaturated carbon atoms, Cx and Cy of the two chains, L1 and L2, respectively and [b] Change in the unsaturated sp^2 hybridized double bond lengths before (normal) and after (italic) the calculations.
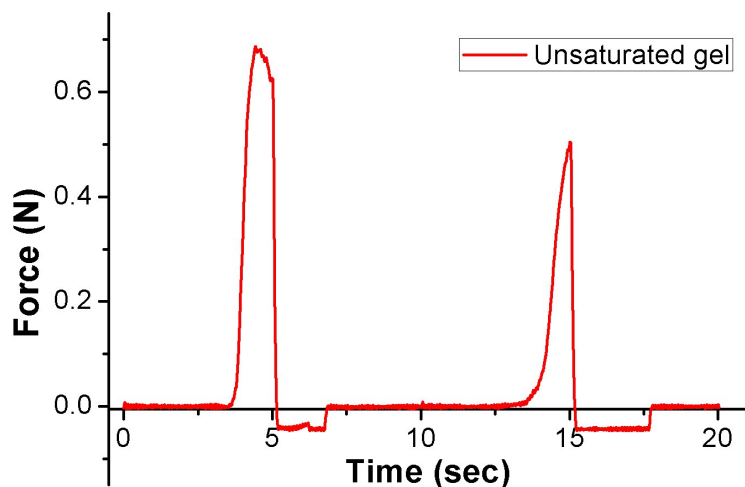
7. Textural profile analysis

Fig. S5. *Two-cycle uniaxial compression test of the NCT gel*

Table S3. Textural parameters of the molecular gels and biopolymeric gels

Type of formulation	Hardness	Cohesiveness (%)	Adhesiveness (N.s)	References
NCTgel, 2 wt%	0.69 N	49	-0.07	--
NPPT gel, 2wt %	--	--		--
Gelatin, 10 wt%	40.08 N		-0.35	4
AMCS*, 10 wt%	1.10 N		-2.08	
Konjac gel#	2.38 N	90		5
Na-Alg*, 3 wt%	1.99 N	--	--	6
HPMC*, 3 wt%	3.37N	--	--	

8. Results and Discussion (DPD Simulation)

The self-assembly of the dynamics behavior of the micelle formation is studied with various simulation steps for NCT system in toluene solution. The mesoscale dynamic simulation is carried out with NCT concentrations from 2-3.3%. Therefore, in the simulation we used the ratio of NCT beads to toluene beads as ~2-3.37:97. The respective mesoscopic appearance of the system is shown in Fig. S8. Initially NCT beads were randomly distributed in toluene solution. With the increase in dynamic time-step, the NCT beads initiate to aggregate into small clusters and subsequently to small worm like micelles (WLMs). As the system approaches the equilibrium state (after 40,000 step), the NCT beads form more smaller WLMs and then long worm micelles, as shown in Fig. S8, and the morphology remains intact.
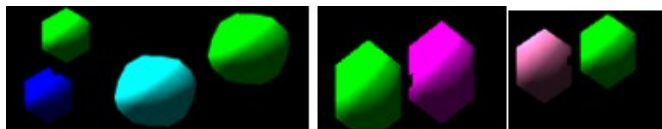
Fig. S6. *Bead description: Tail beads of D0 (Pink), D1 (Blue), D2 (Sky Blue) and D3 (Magneta), Hydrophilic head beads H in Green*
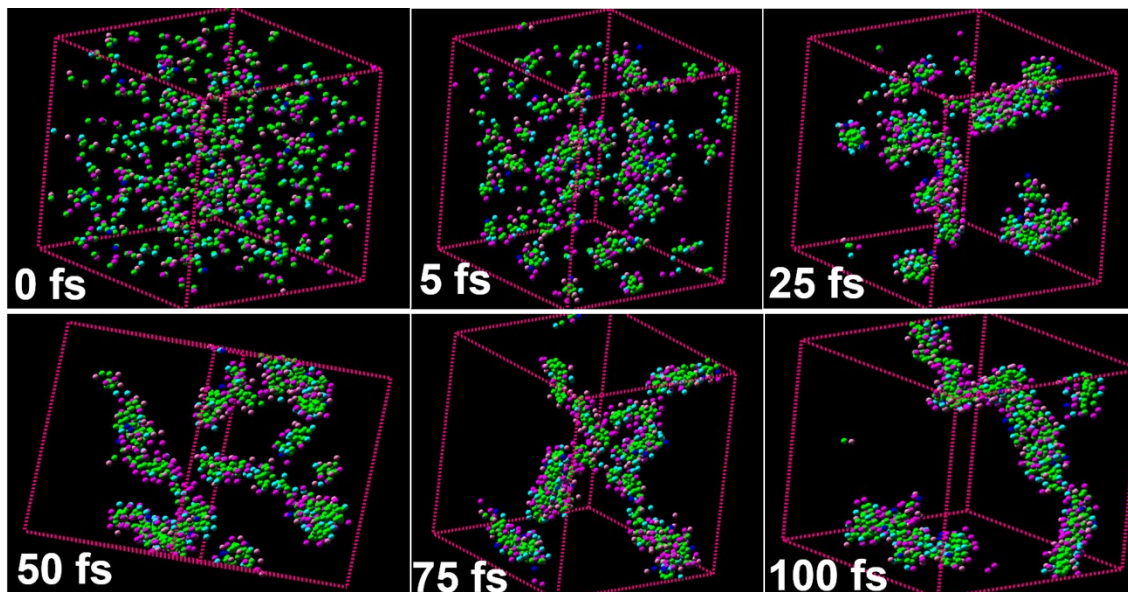

Fig. S7. *Snapshots collected from DPD simulation after different timescales depicting the growth of shorter and longer worm like micelles (periodic boundary conditions 20 X 20 X 20, NCT 2% and Toluene 98%)*
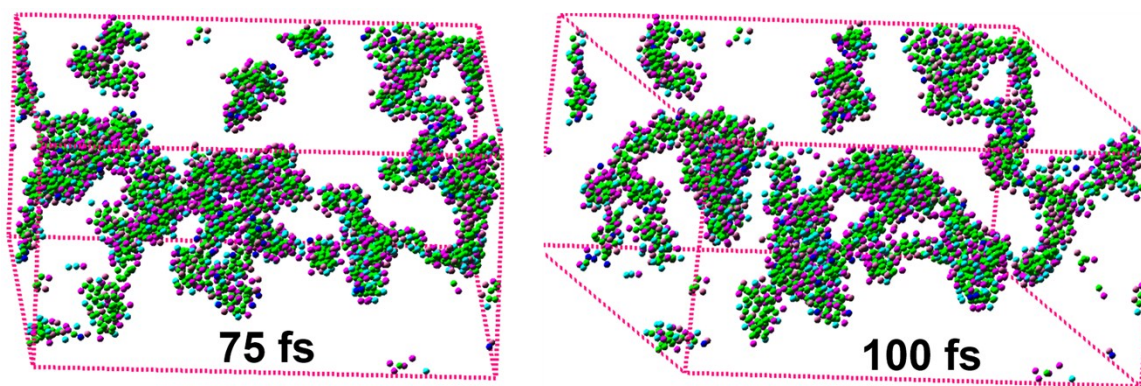

Fig. S8. *Snapshots collected from DPD simulation after different timescales depicting the growth of worm like micelles under periodic boundary conditions 40 X 40 X 20 (NCT 2% and Toluene 98%)*
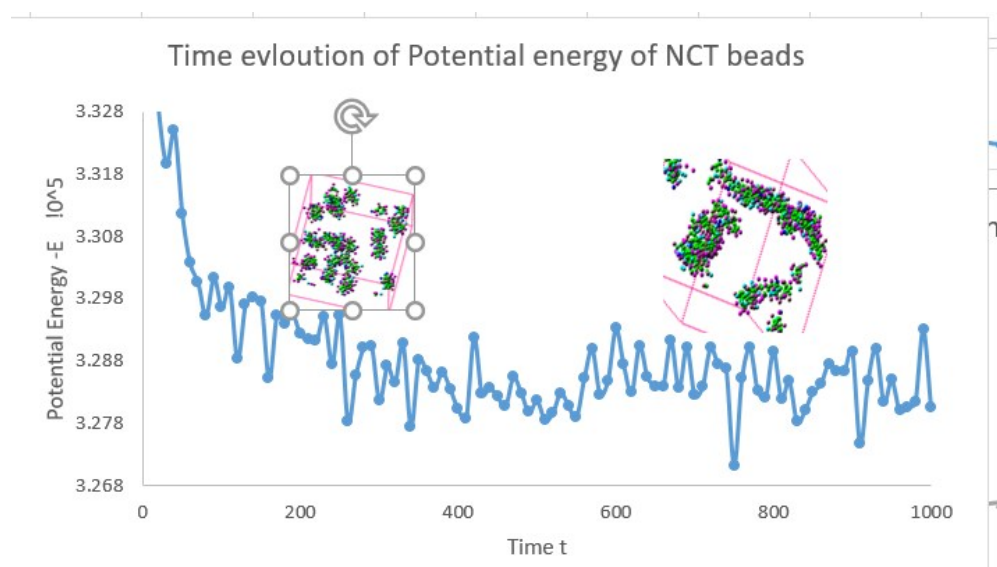
10

Fig. S9. *Time evolution of Potential Energy of toluene-NCT (98:2) system under periodic boundary conditions 20X20X20*
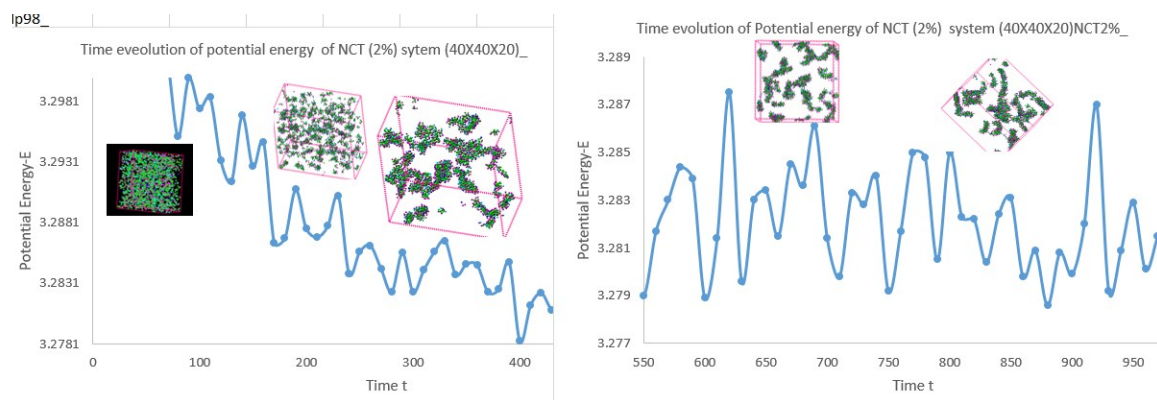

Fig. S10. *Time evolution of Potential Energy of toluene-NCT (98:2) system under periodic boundary conditions 40 X 40 X 20 (left: 0 to 400 time-steps and right: 550 to 1000 time-steps).*

This dynamic assembly process can also be monitored from the change in potential energy of the system with respect to the time-steps, as shown in Fig. S10.
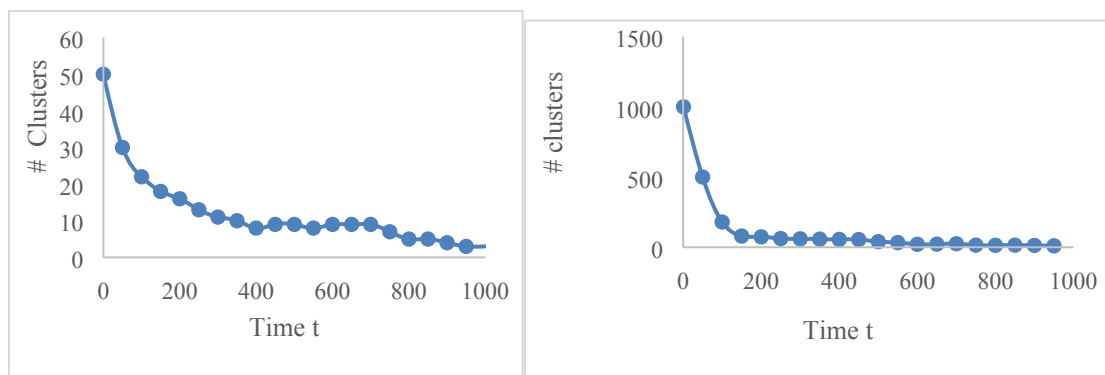
Fig. S11. *Time evolution of number of clusters under boundary conditions 20 X 20 X 20 (left) and 40 X 40 X 20 (right)*

Fig. S11 shows the total potential energy, E and the number of clusters that is formed during the simulation time. The total potential energy decreases rapidly with the decrease in the number of clusters or growth of clusters. However, once the clusters turn into worm-like micelles (WLMs), the change in potential energy becomes almost constant. This indicates that the potential energy is insensitive during the coalescence of smaller cluster into large WLMs formation. The largest approximate size of WLM is in between 14 to 40 Å within or under the dimension of 40 X 40 X 20 boundary condition.

Effect of concentration: As the concentration of the toluene decreased to 96.7%, we observed longer worm like structures due to higher concentration of NCT, as shown in Fig. S12.
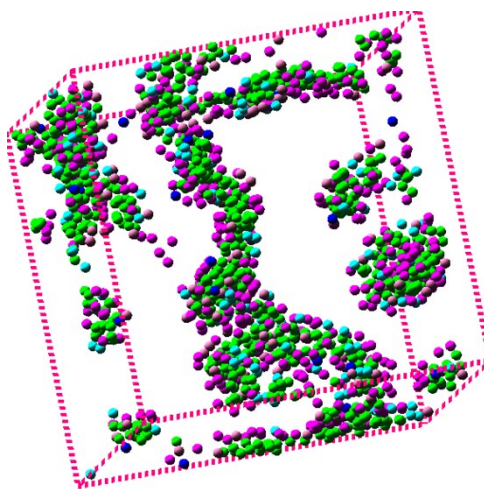

Fig. S12. *Snapshots of the dynamic simulation at 350 time-step in toluene (96.7%) –NCT (3.3%) system. Toluene beads are excluded for clarity*

At t= 350 time step, the longest worm having an approximate contour length is ~38-43 Å, as seen from Fig. S12. The respective kinetic energy for this system is shown below in Fig. S13.
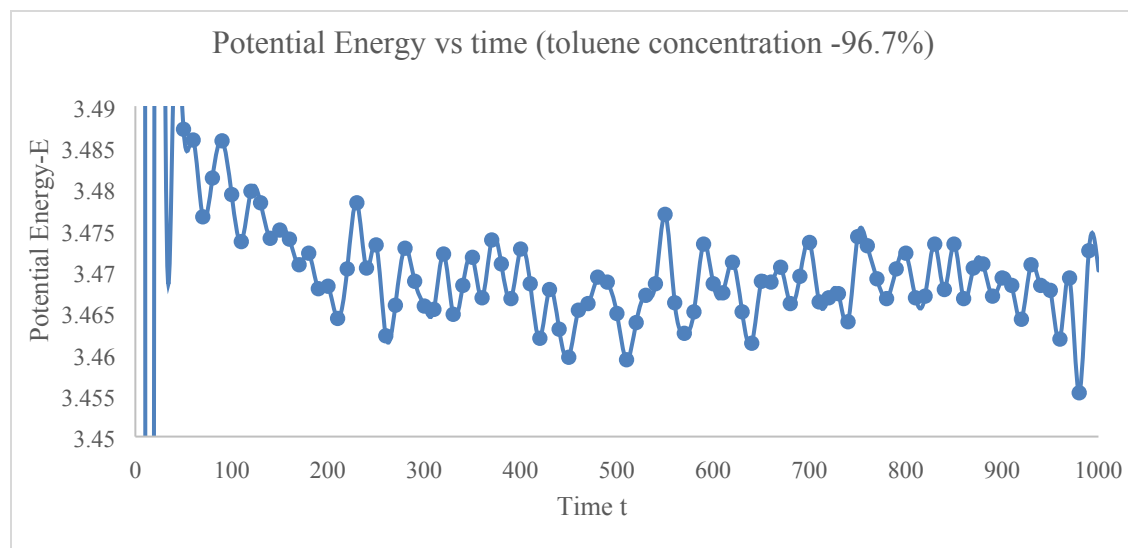
Fig. S13. *Time evolution of potential energy for toluene (96.7%) –NCT (3.3%) system (periodic boundary conditions 20 X 20 X 20)*

9. References

1. J. H. Prestegard, *Nat. Struct. Biol.* **1998,** *5,* 517- 522.
2. M. Rueckert, G. Otting, *J. Am. Chem. Soc*., **2000,** *122,* 7793-7797.
3. J. C. Freudenberger, S. Knoer, K. Kobzar, D. Heckmann, T. Paululat, H. Kessler, B. Luy, *Angew. Chem. Int. Ed*. **2005,** *44,* 423 426.
4. P. H. M. Marfil, A. C. B. M. Anhê, V. R. N. Telis, *Food Biophysics* **2012.** *7*, 236.
5. F. Jiménez-Colmenero, S. Cofrades, A. M. Herrero, F. Fernández-Martín, L. Rodríguez-Salas, C. Ruiz-Capillas, *Food Hydrocolloids* **2012**, *26*, 63.
6. K. Rehman, M. C. I. Mohd Amin, M. H. Zulfakar, *Journal of Oleo Science* **2014.** *63*, 961.
7. V. V. Ginzburg, K. Chang, P. K. Jog, A. B. Argenton, L. Rakesh, *J. Phys. Chem. B*, **2011**, *115*, 4654-4661.
8. S. Plimpton, *J. Comp. Phys.,* **1995***, 11,1.*